Role of grain boundary and grain defects on ferromagnetism in Co:ZnO films

H. S. Hsu and J. C. A. Huang[a)]
Department of Physics, National Cheng Kung University, Tainan, Taiwan 701, Republic of China and Center of Nanoscience and Nanotechnology, National Cheng Kung University, Tainan, Taiwan 701, Republic of China

S. F. Chen and C. P. Liu
Department of Materials Science and Engineering, National Cheng Kung University, Tainan, Taiwan 701, Republic of China

(Received 15 December 2006; accepted 1 February 2007; published online 7 March 2007)

The annealing effects on magnetism, structure, and ac transport for Co:ZnO films have been systematically investigated. The room temperature saturation magnetization (M_s) varies drastically with Ar or Ar/H_2 annealing processes. By using the impedance spectra, the change in grain boundary and grain defects of these films can be analyzed. The results demonstrate that Ar annealing produces mainly the grain boundary defects which cause the enhancement of M_s. Ar/H_2-annealing creates not only grain boundary defects but also the grain defects, resulting in the stronger enhancement of M_s. Ferromagnetism for Co:ZnO films is influenced by both grain boundaries and grain defects. © *2007 American Institute of Physics*. [DOI: 10.1063/1.2711763]

Transition metal (TM)-doped oxides have attracted considerable interest as promising diluted magnetic semiconductors (DMSs) owing to the possibility of inducing room temperature (RT) ferromagnetism for advanced spintronic applications.[1] RT ferromagnetism has been demonstrated in TM-doped oxide in the absence of magnetic precipitates.[2,3] However, poor conductivity in many diluted magnetic oxide implies that the origin of ferromagnetism in oxide DMS could be fundamentally different from the carrier induced ferromagnetism in III-V DMSs such as Mn doped GaAs.[4] Recently, the bound magnetic polaron (BMP) mediated exchange mechanism[5] with charge-compensating oxygen vacancies has been widely used to interpret the magnetic properties in oxide DMSs such as TM-doped TiO_2 system.[6] Besides, some research groups suggested that the magnetic properties of oxide DMSs may depend sensitively on structure defects other than those introduced to maintain charge neutrality.[7–9] For example, grain boundary defects have been proposed in the activation of RT ferromagnetism by aggregation of TM:ZnO nanocrystals under ambient conditions.[9] Within the BMP scheme, the microstructural defects with radii sufficiently large to include enough magnetic dopants may cause good spin alignment of the doped TM.

The influence of annealing in different atmospheres (e.g., oxidizing, reducing atmosphere, or reducing with additional H_2 or Zn vapor)[10–13] on structure and ferromagnetism in Co:ZnO films has been studied by various researchers. The results suggest instead the free carriers but the structural defects such as oxygen vacancies or zinc interstitials are more critical to the ferromagnetism in oxide DMSs films. Nevertheless, the origin of ferromagnetism in TM-doped oxides is still strongly debated. The aim of this work is to correlate the magnetic property with the response from grain boundaries and grains revealed by ac impedance technique for Co:ZnO films annealed under Ar and Ar/H_2 atomsphere. We demonstrate here that both the grain boundary and grain defects play important roles for the ferromagnetism in Co:ZnO.

5% doped Co:ZnO films of about 600 Å were prepared by ion-beam sputtering (IBS) from two separate targets. The samples were grown on sapphire (0001) substrates at RT. IBS technique has been employed to stabilize good oxide DMS with appropriate magnetic doping concentration.[14] After the IBS growth, these films were separately annealed under 1 atm Ar or $Ar(90\%)/H_2(10\%)$ at 250 °C for 1 h. The magnetic property was probed by a commercial superconducting quantum interference device (Quantum Design). Figure 1(a) displays the magnetic hysteresis loops at RT for the as-deposited and the Ar- and Ar/H_2-annealed films. RT ferromagnetism has been observed for these films. The satura-

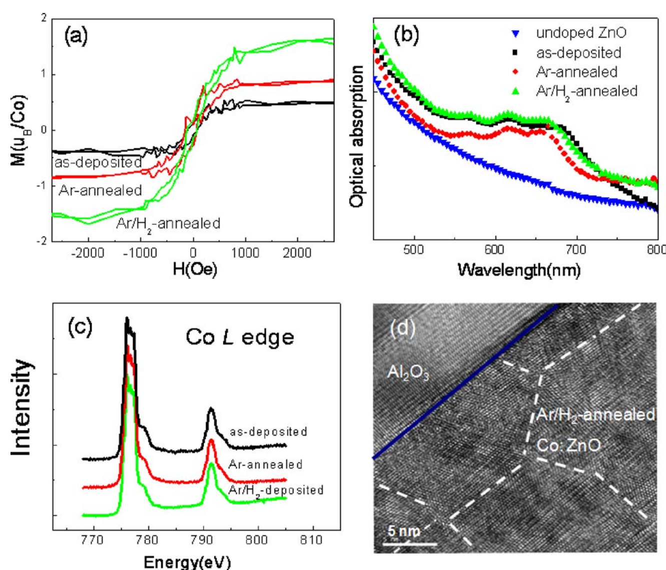

FIG. 1. (Color online) (a) Magnetic hysteresis loops (b) OAS (c) Co $L_{2,3}$ edge XAS spectra of the as-deposited, Ar-annealed, and Ar/H_2-annealed Co:ZnO samples at RT. (d) The HRTEM image for the Ar/H_2-annealed sample. The grain boundaries are indicated by dash lines.

[a)]Electronic mail: jcahuang@mail.ncku.edu.tw

0003-6951/2007/90(10)/102506/3/$23.00 © 2007 American Institute of Physics
Downloaded 27 Sep 2009 to 140.116.208.56. Redistribution subject to AIP license or copyright; see http://apl.aip.org/apl/copyright.jsp

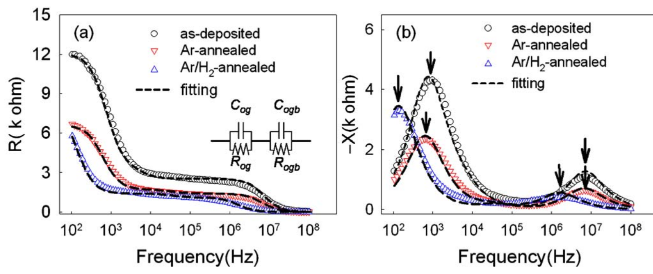

FIG. 2. (Color online) (a) $R(f)$ and (b) $-X(f)$ of CI of the as-deposited, Ar-annealed, and Ar/H_2-annealed Co:ZnO samples. The dash lines were the best fitting results by the equivalent circuit equation. The arrows indicate the local maximums.

tion magnetization (M_s) varied drastically for different annealing processes with $M_s \sim 0.5$, 0.9, and $1.5\mu_B/\text{Co}$ for the as-deposited, Ar-annealed, and Ar/H_2-annealed films, respectively.

To understand the origin of ferromagnetism in oxide DMSs, it is essential to check the formation of any small amount of metal clusters. Figure 1(b) shows the 300 K optical absorption spectra (OAS) of the as-deposited, Ar-annealed, and Ar/H_2-annealed samples with an undoped ZnO (~600 Å) spectrum for comparison. The absorption spectra of the as-deposited films resemble those reported Co^{2+}:ZnO films,[15] showing the characteristic *d-d* band absorption of Co^{2+} ions substitution for the Zn^{2+} sites. The absorption band intensities are expected to be proportional to the Co^{2+} concentration in ZnO films with the same film thicknesses. The similar OASs for the Ar- and Ar/H_2-annealed films clearly show the signature of Co^{2+} in ZnO, indicating that the DMS structure did not decompose under these annealing conditions. Besides, the x-ray absorption spectra (XAS) at Co $L_{2,3}$ edge are provided in the Fig. 1(c). The split line shape feature for all samples also indicates that most of the Co elements are in Co^{+2} valence state with tetrahedral symmetry much as Zn^{2+} in ZnO.[16] Figure 1(d) shows the high resolution transmission electron microscopy (HRTEM) cross-sectional lattice images of the Ar/H_2-annealed sample. No signal of Co clusters has been observed. There are reports suggesting that high temperature (e.g., 450 °C) growth or annealing in Ar/H_2 atmosphere may reduce Co^{2+} to Co^0, thus change M_s and magnetic properties.[13,17] In our cases, however, no detectable Co clusters have been observed because of the relatively lower annealing temperature (250 °C). These results indicate the magnetization enhancement by Ar and Ar/H_2 annealing might be correlated with the microstructural change such as defect variation, as further revealed by the complex impedance (CI).

The CI spectroscopy, the frequency response of the electrical properties, can provide evidence to identify electrical relaxation mechanisms due to grains, grain boundaries, or macroscopic heterogeneities.[18] For example, we have shown that the formation of metallic clusters in TM-doped ZnO films can be identified by bias dependent CI.[19] The CI spectroscopy was carried out by the Hewlett-Packard 4294A impedance analyzer using two-point contact with a fixed oscillating voltage of 0.5 V under dc bias voltage (V_{dc}) from 0 to 1.5 V. The normalized real and imaginary parts of CI, $Z(f)=R(f)+iX(f)$, as a function of frequency for the as-deposited and annealed samples are shown in Fig. 2. For

TABLE I. Fitting parameters from equivalent circuit equation for the time constants of the as-deposited, Ar-annealed, and Ar/H_2-annealed films.

	as-deposited	Ar-annealed	Ar/H_2-annealed
τ_{ogb} (s)	1.68×10^{-4}	2.50×10^{-4}	1.17×10^{-3}
τ_{og} (s)	2.35×10^{-8}	2.38×10^{-8}	9.68×10^{-8}

these samples the real parts $R(f)$ initially decrease, then remain at a certain constant, and are followed by a down step in the frequency range of 10^6-10^8 Hz. In contrast, the negative value of imaginary parts $X(f)$ show two local maxima at specific frequencies (f_{m1}, f_{m2}), which are considered as characteristic peaks corresponding to different types of electrical relaxations. The analyzed results reflect the microstructural properties of the samples. It is noticed that f_{m1} in the low frequency range (1 kHz) for the as-deposited film shifts toward lower frequencies of about 620 and 140 Hz for the Ar-annealed and Ar/H_2-annealed films, respectively. In addition, f_{m2} is much lower for the Ar/H_2-annealed sample (~1.6 MHz) compared to the Ar-annealed (~7 MHz) and as-deposited films (~7 MHz). By f_{m1} and f_{m2}, the relaxation time (τ) of the dynamic response can be determined ($\tau=1/2\pi f$). The variation of f_{m1} and f_{m2} for $-X(f)$ can be characterized as the microstructure change of Co-doped ZnO films under different annealing processes as discussed below.

The equivalent circuit (EC) composed of resistance (R) and capacitance (C) elements has been utilized in the CI analysis. Based on the impedance results, two sets of parallel RC components in series [as illustrated in Fig. 2(a)] have been employed to model the CI spectra

$$Z = R + iX = (1/R_{ogb} + i\omega C_{ogb})^{-1} + (1/R_{og} + i\omega C_{og})^{-1}, \quad (1)$$

where R_{ogb} and C_{ogb} represent the R and C from the oxide grain boundary dominated in the low frequency regime and R_{og} and C_{og} represent the oxide grain contribution dominated in the high frequency regime. The dash curves in Fig. 2 are obtained by the best fits of the experimental data, which reveal good agreement of the EC model with the CI spectra. The relaxation time ($\tau=RC$), an intrinsic characteristic property of the materials, can thus be obtained from the fitting parameters. For convenience of the readers, the fitting time constants τ for these films are summarized in Table I. These values are consistent with the time constants determined by f_{m1} and f_{m2}.

Since the time constant τ depends sensitively on the abundance of defects in the grain boundaries and grains, CI analysis can be used to characterize the influence of defects on dielectric relaxation. The oxide samples generally contain more defects such as oxygen vacancies or metallic interstitials among the nonstoichiometric grain boundaries. Therefore the grain boundaries exhibit slower relaxation behavior than the grains. Generally the relaxation time constant due to oxide grain boundaries (τ_{ogb}) is larger than the time constant due to oxide grains (τ_{og}) by at least two orders of magnitude.[20] For these Co-doped ZnO films, the τ_{ogb} are in the order of $10^{-3}-10^{-4}$ s, as fitted by the EC model. The Ar/H_2-annealed film reveals the slowest relaxation (largest τ_{ogb}) due likely to more grain boundary defects and the as-deposited sample shows the fastest relaxation (smallest τ_{ogb}) with less grain boundary defects. This result is attributed to the gain of structural defects (oxygen vacancies or Zn inter-

Downloaded 27 Sep 2009 to 140.116.208.56. Redistribution subject to AIP license or copyright; see http://apl.aip.org/apl/copyright.jsp

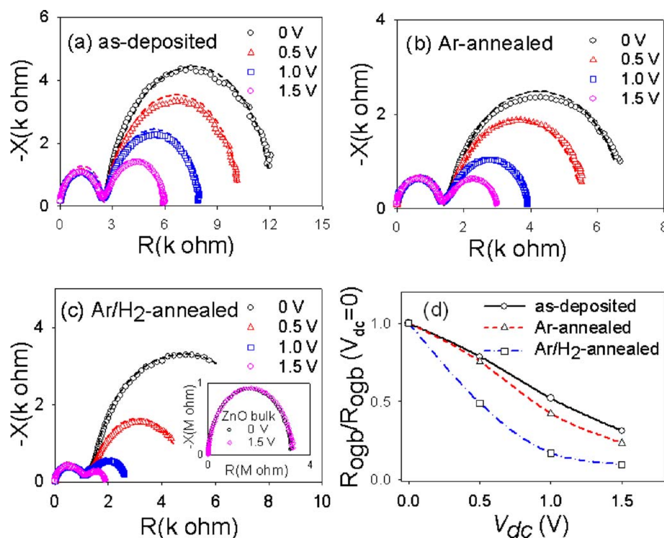

FIG. 3. (Color online) Nyquist plots for the (a) as-deposited, (b) Ar-annealed, and (c) Ar/H_2-annealed Co-doped ZnO samples at various V_{dc} (open circles) and fitting results (dash curves). (d) The variations of the fitting parameters for $R_{ogb}/R_{ogb}(V_{dc}=0)$ as a function of the V_{dc}. The lines in (d) are guides for the eyes.

stitials) from ZnO grain boundaries by annealing. It is expected that Ar/H_2 annealing would create more defects in grain boundaries than Ar annealing process. Therefore, the τ_{ogb} of the Ar/H_2-annealed film is almost one order of magnitude larger than the other films. In addition, the τ_{og} of these samples are in the order of 10^{-8} s. The τ_{og} of Ar/H_2-annealed film is about triple of the Ar-annealed and as-deposited films. We speculate that for the Ar/H_2-annealed sample, hydrogens are able to diffuse into the grains interior and create more defects, while for the Ar annealing process the defects are created mainly in the grain boundaries.

To further explore these films, an additional V_{dc} has been adopted to the CI measurements. Figure 3 shows the bias dependent Nyquist plots of $-X$ vs R for the as-deposited and annealed samples together with a ZnO bulk sample in the inset of Fig. 3(c). For the Co:ZnO films, two semicircles in Nyquist plots corresponding to the electrical relaxation by grains and grain boundaries have been observed. The V_{dc} study reveals that the bias dependent term (in low frequency regime) corresponds to the grain boundaries contribution, and the bias independent term (in high frequency regime) relates to the grains contribution. In contrast, the Nyquist plots for the bulk ZnO samples only reveal voltage independent, single semicircle which corresponds to only grain interior contribution. The results suggest that the observed CI spectra likely reflect the defect variation between the polycrystalline Co:ZnO films and bulk ZnO sample. The CI results of the Co:ZnO films with V_{dc} from 0 to 1.5 V can also be well fitted by the Eq. (1), as illustrated by the dashed curves in Fig. 3. The analyzing results show that both the C_{og} and C_{ogb} are independent on V_{dc}.[18] On the other hand, R_{ogb} decreases with increasing V_{dc}, whereas R_{og} is almost independent of V_{dc}. The decrease of R_{ogb} with increasing V_{dc} can be related to defects created in the grain boundaries, which can result in trap states and provide more conducting channels. Therefore, one can qualitatively determine the defect density in grain boundaries among these samples by the bias-voltage dependence R_{ogb}. The normalized R_{ogb} of the as-deposited, Ar-annealed, and Ar/H_2-annealed samples are plotted as a function of V_{dc}, as shown in Fig. 3(d). Obviously, the annealing treatment changes the V_{dc} dependence of R_{ogb}, especially for the samples annealed under Ar/H_2 atmosphere. This result could also reveal the defect density variation among grain boundaries for these samples.

To summarize, the fluctuation of magnetization in the Co:ZnO films can be attributed to the variation of microstructural defects tuned by distinct annealing conditions. The Ar-annealing process produces mainly grain boundary defects which cause partial enhancement of ferromagnetism. The Ar/H_2 annealing process promotes not only the grain boundary defects but also the grain defects which result in stronger enhancement of M_s. We demonstrate that the formation of defects in grains and grain boundaries shall be considered for the microstructural origin of ferromagnetism for oxide DMSs.

This work has been supported by National Science Council of the ROC under Grant No. NSC 95-2120-M-006-004.

[1]S. J. Pearton, C. R. Abernathy, M. E. Overberg, G. T. Thaler, D. P. Norton, N. Theodoropoulou, A. F. Hebard, Y. D. Park, F. Ren, J. Kim, and L. A. Boatner, J. Appl. Phys. **93**, 1 (2003).
[2]T. Zhao, S. R. Shinde, S. B. Ogale, H. Zheng, T. Venkatesan, R. Ramesh, and S. Das Sarma, Phys. Rev. Lett. **94**, 126601 (2005).
[3]Z. Yin, N. Chen, C. Chai, and F. Yang, J. Appl. Phys. **96**, 5093 (2004).
[4]T. Dietl, H. Ohno, F. Matsukura, J. Cibert, and D. Ferrand, Science **287**, 1019 (2000).
[5]J. M. D. Coey, M. Venkatesan, and C. B. Fitzgerald, Nat. Mater. **4**, 173 (2005).
[6]K. A. Griffin, A. B. Pakhomov, C. M. Wang, S. M. Heald, and K. M. Krishnan, Phys. Rev. Lett. **94**, 157204 (2005).
[7]T. C. Kaspar, S. M. Heald, C. M. Wang, J. D. Bryan, T. Droubay, V. Shutthanandan, S. Thevuthasan, D. E. McCready, A. J. Kellock, D. R. Gamelin, and S. A. Chambers, Phys. Rev. Lett. **95**, 217203 (2005).
[8]N. H. Hong, J. Sakai, N. T. Huong, N. Poirot, and A. Ruyter, Phys. Rev. B **72**, 045336 (2005).
[9]J. D. Bryan, S. A. Santangelo, S. C. Keveren, and D. R. Gamelin, J. Am. Chem. Soc. **126**, 11640 (2004).
[10]N. Khare, M. J. Kappers, M. Wei, and M. G. Blamire, Adv. Mater. (Weinheim, Ger.) **18**, 1449 (2006).
[11]K. R. Kittilstved, D. A. Schwartz, A. C. Tuan, S. M. Heald, S. A. Chambers, and D. R. Gamelin, Phys. Rev. Lett. **97**, 037203 (2006).
[12]H. S. Hsu, J. C. A. Huang, Y. H. Huang, Y. F. Liao, M. Z. Lin, C. H. Lee, J. F. Lee, S. F. Chen, L. Y. Lai, and C. P. Liu, Appl. Phys. Lett. **88**, 242507 (2006).
[13]H. J. Lee, C. H. Park, S.-Y. Jeong, K.-J. Yee, C. R. Cho, M.-H. Jung, and D. J. Chadi, Appl. Phys. Lett. **88**, 062504 (2006).
[14]J. C. A. Huang, H. S. Hsu, Y. M. Hu, C. H. Lee, Y. H. Huang, and M. Z. Lin, Appl. Phys. Lett. **85**, 3815 (2004).
[15]P. Koidl, Phys. Rev. B **15**, 2493 (1977).
[16]B. J. Kim, S. Yoon, B. J. Suh, S. W. Han, K. H. Kim, K. J. Kim, B. S. Kim, H. J. Song, H. J. Shin, J. H. Shim, and B. I. Min, Appl. Phys. Lett. **84**, 4233 (2004).
[17]S. Deka and P. A. Joy, Appl. Phys. Lett. **89**, 032508 (2006).
[18]A. K. Jonscher, Nature (London) **264**, 673 (1977).
[19]J. C. A. Huang and H. S. Hsu, Appl. Phys. Lett. **87**, 132503 (2005).
[20]J. R. Macdonald, *Impedance Spectroscopy Emphasizing Solid Materials and Systems* (Wiley, New York, 1987), Chap. 4, p. 40.

Downloaded 27 Sep 2009 to 140.116.208.56. Redistribution subject to AIP license or copyright; see http://apl.aip.org/apl/copyright.jsp